

Relativistic hybrid stars with super-strong toroidal magnetic fields: An evolutionary track with QCD phase transition

Nobutoshi Yasutake^{1*}, Kenta Kiuchi^{2†}, Kei Kotake^{1,3‡}

¹*Division of Theoretical Astronomy, National Astronomical Observatory of Japan, 2-21-1 Osawa, Mitaka, Tokyo 181-8588, Japan*

²*Department of Physics, Waseda University, 3-4-1 Okubo, Shinjuku-ku, Tokyo 169-8555, Japan*

³*Center for Computational Astrophysics, National Astronomical Observatory of Japan, 2-21-1, Osawa, Mitaka, Tokyo, 181-8588, Japan*

Typeset 23 November 2018; Accepted

ABSTRACT

We investigate structures of hybrid stars, which feature quark core surrounded by a hadronic matter mantle, with super-strong toroidal magnetic fields in full general relativity. Modeling the equation of state (EOS) with a first order transition by bridging the MIT bag model for the description of quark matter and the nuclear EOS by Shen et al., we numerically construct thousands of the equilibrium configurations to study the effects of the phase transition. It is found that the appearance of the quark phase can affect distributions of the magnetic fields inside the hybrid stars, making the maximum field strength about up to 30 % larger than for the normal neutron stars. Using the equilibrium configurations, we explore the possible evolutionary paths to the formation of hybrid stars due to the spin-down of magnetized rotating neutron stars. We find that the energy release by the phase transition to the hybrid stars is quite large ($\lesssim 10^{52}$ erg) even for super strongly magnetized compact stars. Our results suggest that the strong gravitational-wave emission and the sudden spin-up signature could be observable signals of the QCD phase transition, possibly for a source out to Megaparsec distances.

Key words: dense matter – equation of state – gravitation – stars: rotation – stars:neutron

1 INTRODUCTION

A very hot issue in hadronic and nuclear physics is to search the phase transition from baryons to their constituents - deconfined quarks. Heavy ion colliders such as RHIC (Brookhaven) and LHC (CERN) are now on line to explore the QCD phase diagram for the high temperature and small baryon density regimes, for which lattice QCD calculations predict a smooth crossover to the QCD phase transition (see Stephanov (2004) for review).

Conversely for the low temperature and high baryon density regimes, compact stars are expected to provide a unique window on the phase transition at their extreme density with super-strong magnetic field. It has been suggested long ago that quark matter may exist in the interior of compact objects (Itoh 1970; Bodmer 1971; Witten 1984). Hybrid stars (and strange quark stars) are considered to be such objects, which feature quark cores surrounded by a hadronic

matter mantle (or quark cores only) (for reviews, e.g., Weber (1999); Glendenning (2001)). Even if the relevant conditions could be reached in a laboratory in the near future (Senger 2004), the conditions prevailing in the compact stars are different from those produced in accelerators, i.e., the matter is long-lived, charge neutral and in β -equilibrium with respect to weak interactions. It is therefore important to investigate the properties of such “exotic” stars, providing hints about the main features of matter at those extreme conditions.

The formation of the quark cores in compact stars is expected to take place by a first-order phase transition (Glendenning 1992, 2001). Albeit still very uncertain (e.g., Horvath (2007)), such a transition would proceed by the conversion of initially metastable hadronic matter in the core into the new deconfined quark phase. The metastable phase could be formed as the central density of neutron stars exceeds a critical value, due to mass accretion, spin-down or cooling. Possible astrophysical sites are in the protoneutron stars during the collapse of supernova cores (near the epoch of bounce (Takahara & Sato 1985; Yasutake et al. 2007) or at the late postbounce phase (Gentile et al. 1993;

* E-mail: yasutake@th.nao.ac.jp

† kiuchi@gravity.phys.waseda.ac.jp

‡ kei.kotake@nao.ac.jp

Nakazato et al. 2008; Sagert et al. 2008)) and in old neutron stars accreting from their companions (Benvenuto et al. 1994; Chau 1997; Lin et al. 2006). In whichever cases, the sudden nucleation of the exotic phase in the hadronic star will be accompanied by a core-quake and huge energy release of the gravitational binding energy. Such energy release has been proposed to explain the central engines of the gamma-ray bursts (Bombaci & Datta 2000; Berezhiani et al. 2003). Possible observables of these transient phenomenon should be glitches, magnetar flares, and superbursts (Alford et al. 2007). In addition, the detection of gravitational waves (Ioka 2001; Yasutake et al. 2007; Lin et al. 2006; Abdikamalov et al. 2008) and neutrinos (Nakazato et al. 2008; Sagert et al. 2008) generated at the moment of the phase transition, should supply us implications to unveil the mechanism of the phase transition.

Here it should be noted that most of these calculations/estimations concerning the phase transition inside compact stars are limited to a non-rotating case, in which the Tolman-Oppenheimer-Volkoff equation is solved to obtain their structures (Haensel et al. 1986; Zdunik et al. 1987; Muto & Tatsumi 1990; Drago et al. 2004; Yasutake & Kashiwa 2009). Exceptions are for Gourgoulhon et al. (1999); Yasutake et al. (2005); Zdunik et al. (2007), in which relativistic equilibrium configurations of rotating strange stars, beyond the so-called slow rotation approximations (see references in Glendenning (2001)), are constructed for estimating the energy release. In Gourgoulhon et al. (1999); Yasutake et al. (2005), hadron matter is assumed to be converted fully to quark matter, leading to the formation of strange quark stars like in Alcock et al. (1986); Benvenuto & Horvath (1989); Olesen & Madsen (1991); Lugones et al. (1994). However, it is recently pointed out that the strange quark stars could be ruled out by their too fast spin-down rates via gravitational radiations from r-modes instability (Madsen 2000). The quasi-periodic oscillations (QPOs) of strange quark stars could not be reconciled with the observations (Watts & Reddy 2007). Moreover, Mallick et al. (2009) has recently claimed that magnetars cannot convert to purely quark stars, but only to hybrid stars. These suggest us to pay attention to hybrid stars rather than stars made of purely deconfined quarks. In a very recent work by Zdunik et al. (2008), the phase transition of rotating hybrid stars is discussed, however, the equation of state (EOS) is made very idealistic, assumed to model a strong phase transition, seemingly less sophisticated than the EOSs in the recent literature cited above. In addition to rotation, neutron stars observed in nature are magnetized with the typical magnetic field strength $\sim 10^{11}$ – 10^{13} G (Lyne & Graham-Smith 2005). The field strength is often much larger than the canonical value as $\sim 10^{15}$ G for a special class of the neutron stars such as magnetars (Lattimer & Prakash 2007; Woods & Thompson 2006). In a series of our recent papers (Kiuchi & Kotake 2008; Kiuchi & Yoshida 2008; Kiuchi et al. 2008d), we have studied equilibrium configurations of relativistic magnetized compact stars to apply for the understanding of their formations and evolutions, but with hadronic EOSs.

Above situations motivate us to investigate the structures of relativistic hybrid stars with magnetic fields, and by using them, to estimate the energy release at the phase

transition. This study is posed as an extension to the study by Yasutake et al. (2005), in which the phase transition to the rotating strange stars was investigated. Due to the unavailability of the method to construct a fully general relativistic star with arbitrarily magnetic structures (namely both with toroidal and poloidal fields), we here consider the equilibrium with purely toroidal fields as in Kiuchi & Yoshida (2008). It is noted that the outcomes of the recent stellar evolution calculations (Heger et al. 2005) and the MHD(magnetohydrodynamics) simulations of core-collapse supernovae (Kotake et al. (2004); Takiwaki et al. (2004); Obergaulinger et al. (2006); Dessart et al. (2007); Sawai et al. (2008); Kiuchi et al. (2008c); Takiwaki et al. (2009)), suggesting much dominance of the toroidal fields, are not in contradiction with the assumption. Following the scenario proposed in Yasutake et al. (2005), we consider the possible evolutionary tracks of a rapidly rotating and magnetized neutron star to a slowing rotating hybrid star due to the spin-down via gravitational radiation and/or magnetic braking. During the evolutions, the baryon mass and the magnetic field strength are taken to be constant for simplicity. The energy release can be estimated from the difference in the mass-energies between the hadronic star and the hybrid star along each sequence. By constructing thousands of equilibrium configurations, we hope to clarify the possible maximum energy release at the moment of the transition and discuss their astrophysical implications.

The paper is organized as follows. The method for constructing the EOS with the phase transition and the numerical scheme for the stellar equilibrium configurations are briefly summarized in Sec. 2. Sec. 3 is devoted to showing numerical results. Summary and discussion follow in Sec. 4. In this paper, we use geometrical units with $G = c = 1$.

2 EQUATION OF STATE AND NUMERICAL METHOD

2.1 Equations of State with a first-order phase transition

As mentioned, we assume that the deconfinement of the quarks takes place at the first order phase transition. In this case, a mixed phase can form and it is typically described using two separate EOSs, one for the hadronic and the other for the quark phase. Here the bulk Gibbs construction is used to bridge the two phases. In the following, we briefly summarize the adopted EOSs for each phase and explain the features of the resulting EOS with the first order phase transition.

Since lattice QCD is yet to make solid predictions for large density regimes in compact objects, the quark matter EOS is currently computed using phenomenological descriptions such as the MIT bag or the Nambu-Jona-Lasinio (NJL) models. For the quark phase, we choose the EOS based on the very simple but widely applied MIT bag model (see Weber (1999); Glendenning (2001) for reviews). Using the model, one can express the energy density, ϵ , and the pressure, P of strange quark matter as functions of baryon number density, n in the following form,

$$\epsilon = \sum_f \epsilon_f + B, \quad (1)$$

$$\epsilon_f = \frac{3m_f^4}{8\pi^2} [x_f(2x_f^2 + 1)\sqrt{1 + x_f^2} - \operatorname{arsinh} x_f], \quad (2)$$

$$P = n^2 \frac{d(\epsilon/n)}{dn}, \quad (3)$$

where m_f is the quark mass of the flavor of f taken to be $m_u = m_d = 5$ MeV and $m_s = 150$ MeV, $x_f = k_F^{(f)}/m_f$ is a normalized Fermi wave number of $k_F^{(f)}$, and B is the bag constant. Baryon number density of strange matter is $n = \frac{1}{3}(n_u + n_d + n_s)$, where $n_f = k_F^{(f)3}/\pi^2$ is the number density of f quarks. We use a simple MIT bag model of self-bound strange quark matter (Chodos et al. 1974), neglecting the quark interactions except for the confinement effects described by the bag constant (see, e.g., references in Bonanno et al. (2007) for sophistication of the model). We set that the bag constants are 200 MeV fm^{-3} and 250 MeV fm^{-3} in this paper. These values seem consistent with the implications in the recent lattice QCD results (Ivanov et al. 2005). The quark EOS with lower bag constant than 200 MeV fm^{-3} may be too soft to be compatible with the observation of the massive neutron star like pulsars Ter 5 I and J ($> 1.68M_\odot$ with 95 % confidence) (Ransom et al. 2005; Alford et al. 2007). For the EOS of the hadron phase, we adopt the nuclear EOS developed by Shen et al. (1998), which are often employed in recent MHD simulations relevant for magnetars (see Kotake et al. (2006) for a review). The Shen EOS is based on the relativistic mean field theory with a local density approximation, which has been constructed to reproduce the experimental data of masses and radii of stable and unstable nuclei (see references in Shen et al. (1998)). At the maximum densities higher than two times of saturation density, muons may appear (Wiringa et al. 1988; Akmal et al. 1998). However, we neglect it, since the muon contribution to pressure at the higher density has been pointed to be very small (Douchin & Haensel 2001).

In modeling the phase transition to quark matter, there is a main physical uncertainty, the critical density for the onset of the mixed phase. Under the MIT bag model, the transition is determined by the value of the bag constant. We use the bulk Gibbs construction to bridge the two phases using the technique developed by Glendenning (1992). In the transition, two conserved quantities are the baryon number density (n_B) and the electric charge density ($: Y_e n_B$ with Y_e being the electron fraction),

$$n_B = \chi n_{B,Q} + (1 - \chi) n_{B,H}, \quad (4)$$

$$Y_e n_B = \chi Y_{C,Q} n_{B,Q} + (1 - \chi) Y_{C,H} n_{B,H}. \quad (5)$$

Here χ is the volume fraction of matter in the quark phase. The subscripts H and Q label the number density and the charge fraction, Y_C , in the hadronic and in the quark phase, respectively. Since matter in cold compact stars is in chemical equilibrium under β -decay with vanishing neutrino chemical potentials, the following equations have to be satisfied,

$$\mu_e + \mu_p = \mu_n, \quad (6)$$

$$\mu_n = \mu_u + 2\mu_d, \quad (7)$$

$$\mu_p = 2\mu_u + \mu_d, \quad (8)$$

$$\mu_d = \mu_s, \quad (9)$$

together with the mechanical equilibrium, the equality of

the pressure in the two phases,

$$P^Q = P^H. \quad (10)$$

Here for simplicity, the finite size effects on the phase transition (Endo et al. 2006; Maruyama et al. 2006) are ignored. Five unknown variables to describe the mixed phase ($\chi, n_{B,Q}, n_{B,H}, Y_{C,Q}, Y_{C,H}$) can be solved by the five sets of the equations of (3,4,6,7,9).

Figures 1 and 2 show the constructed EOS with the first-order phase transition. For comparison, we also plot the hadronic ‘‘Shen EOS’’ mentioned above and pure quark EOS (‘‘quarkB200’’ and ‘‘quarkB250’’). The left and right panels are the pressure and the energy per baryon as a function of the baryon density, respectively. The labels of ‘‘mixB200(quarkB200)’’ and ‘‘mixB250(quarkB250)’’ indicate the two different bag constants, $B=200 \text{ MeV fm}^{-3}$ and 250 MeV fm^{-3} . The EOS consists of the three phases of the ‘‘Hadron’’, ‘‘Mixed’’, and the ‘‘Quark’’. The critical densities with n_1 (open circles) and n_2 (closed circles) marking the boundaries between the hadron, mixed, and quark phase, are also given in Table 1. From the left panel and Table 1, it can be seen that the critical density for the mixed phase becomes higher for the larger bag constant. This is because for the large bag constant, the density should be larger to achieve the equilibrium between the mixed phase and the pure hadron phase, remembering that the pressure of the quark matter becomes smaller with increasing the bag constant (from Eqs. (1,2)). The higher n_1 for the large bag constant also leads to the higher n_2 , the transition to the quark phase (Table 1). From the right panel of Figure 1 and 2, it is seen that the energy with the quark phase (‘‘mixB200’’ and ‘‘mixB250’’) are clearly lower than the case only with the hadronic phase (‘‘shen’’), and also that the energy is generally lower for the smaller bag constant above n_1 .

The actual conversion process from nuclear matter to quark matter has been of a topic of hot debate, such as detonation or deflagration (Drago et al. 2007). The range of the conversion timescale is estimated to be very wide, roughly $0.1 - 100$ sec, depending upon the bag constant, temperature, mass of neutron stars, and so forth (Olesen & Madsen 1991). Since our main aim of this paper is the estimation of the liberated energy by the conversion from neutron stars to hybrid stars, we do not consider the detailed combustion processes in this study.

Proto-neutron stars left after supernova explosion are very hot (~ 50 MeV) initially, however, cool down below ~ 1 MeV in some tens of seconds (Burrows & Lattimer 1986). The newly formed neutron stars stabilize at practically zero temperature. As mentioned, in cold neutron stars, the β equilibrium in the weak interactions can be well validated, with neutrinos and antineutrinos freely escaping from the star. Combining the zero-temperature, zero-neutrino fraction, and the beta-equilibrium conditions with the charge neutrality condition, the thermodynamic variables depending on the three parameters (e.g. the pressure as $P(\rho, Y_e, T)$ with Y_e being the electron fraction), can only be determined by a single variable (barotropic), which we take to be the energy density, namely $P(\epsilon)$ (Shapiro & Teukolsky 1983) in the following.

In the following, we introduce the baryon mass density, ρ_0 , for convenience, defined to be the number density, n , multiplied a baryon mass, $m_0 = 1.6605 \times 10^{-24}$ g.

Table 1. Critical densities making the transition to the mixed, n_1 , and the quark phase, n_2 , respectively.

EOS	n_1 [/fm ³]	n_2 [/fm ³]
mixB200	2.30E-01	1.29
mixB250	2.63E-01	1.51

2.2 Constructing method of equilibrium stellar configurations

Employing the constructed EOS with the phase transition, we construct the equilibrium stellar configurations. As mentioned in introduction, we pay attention to the general relativistic and toroidally magnetized stellar configurations. The basic equations and the numerical methods for the purpose are already given in Kiuchi & Yoshida (2008). Hence, we only give a brief summary for later convenience.

Assumptions to obtain the equilibrium models are summarized as follows ; (1) Equilibrium models are stationary and axisymmetric. (2) The matter source is approximated by a perfect fluid with infinite conductivity. (3) There is no meridional flow of the matter. (4) The EOS for the matter is barotropic, which is satisfied as mentioned. (5) Magnetic axis and rotation axis are aligned. Because the circularity condition (Wald 1984) holds under these assumptions, the metric can be written in the form (Komatsu et al. 1989; Cook et al. 1992),

$$ds^2 = -e^{\gamma+\rho} dt^2 + e^{2\alpha} (dr^2 + r^2 d\theta^2) + e^{\gamma-\rho} r^2 \sin^2 \theta (d\varphi - \omega dt)^2, \quad (11)$$

where the metric potentials, γ , ρ , α , and ω , are functions of r and θ only. We see that the non-zero component of Faraday tensor $F_{\mu\nu}$ in this coordinate is F_{12} . Integrability of the equation of motion of the matter requires,

$$e^{\gamma-2\alpha} \sin \theta F_{12} = K(u); \quad u \equiv \rho_0 h e^{2\gamma} r^2 \sin^2 \theta, \quad (12)$$

where K is an arbitrary function of $\rho_0 h e^{2\gamma} r^2 \sin^2 \theta$. The variables ρ_0 and h represent the baryon density and relativistic specific enthalpy, respectively. Integrating the equation of motion of the matter, we arrive at the equation of hydrostatic equilibrium,

$$\int_0^{P(\epsilon)} \frac{dP}{\epsilon + P} + \frac{\rho + \gamma}{2} + \frac{1}{2} \ln(1 - v^2) + \frac{1}{4\pi} \int \frac{K(u)}{u} \frac{dK}{du} du = C, \quad (13)$$

where $v = (\Omega - \omega)r \sin \theta e^{-\rho}$ with Ω being the angular velocity of the matter and C is an integration constant. Here, we assume the rigid rotation. The first term of equation (13) depends only on EOSs. Hence, we prepare the values of the integral with EOS tables, precisely. This preparation enable us to calculate equation (13) precisely, though our EOSs are quite different from polytrope models. To compute specific models of the magnetized stars, we need specify the function form of K , which determines the distribution of the magnetic fields. We take the following simple form,

$$K(u) = bu^k, \quad (14)$$

where b and k are constants. Regularity of toroidal magnetic field on the magnetic axis requires that $k \geq 1$. If $k \geq 1$, the magnetic fields vanish at the surface of the star. In this study, we consider the $k = 1$ case because in the general relativistic MHD simulation, Kiuchi et al. (2008c) have found that magnetic distribution with $k \neq 1$ is unstable against axisymmetric perturbations.

To solve the master equations numerically, we employ the Cook-Shapiro-Teukolsky scheme (Cook et al. 1992) extended by Kiuchi & Yoshida (2008), which does not care about the function form of EOS. Hence, it is straight forward to update our numerical code for incorporating the EOS with the phase transition.

After obtaining solutions, it is useful to compute global physical quantities characterizing the equilibrium configurations to clearly understand the properties of the sequences of the equilibrium models. In this paper, we compute the following quantities: the gravitational mass M , the baryon rest mass M_0 , the total angular momentum J , the total rotational energy T , the total magnetic energy H , the magnetic flux Φ , the gravitational energy W and the mean deformation rate \bar{e} , whose definitions are explicitly given in Kiuchi & Yoshida (2008). More explicitly, the mean deformation rate \bar{e} is defined as

$$\bar{e} \equiv \frac{I_{zz} - I_{xx}}{I_{zz}}, \quad (15)$$

where $I_{xx} = \pi \int \epsilon r^4 \sin \theta (1 + \cos^2 \theta) dr d\theta$ and $I_{zz} = 2\pi \int \epsilon r^4 \sin^3 \theta dr d\theta$ with ϵ being the energy density of the matter. Circumferential radius R_{cir} is defined as $R_{\text{cir}} \equiv e^{(\gamma-\rho)/2} r_e$ with r_e being the coordinate radius at the stellar equatorial surface.

We checked the convergence of the presented results by doubling the mesh numbers from the standard set of radial and angular direction mesh points of 400×260 . By checking the relativistic virial identities (Bonazzola & Gourgoulhon 1994) for all the models, we confirm that the typical values are orders of magnitude 10^{-3} , and become 10^{-2} at worse (10^{-4} at best). These values, which is a measure of the numerical convergence, are almost same for the polytropic EOS case (Kiuchi & Yoshida 2008). In general, the convergence is known to become much worse for realistic EOSs, because their density and pressure profile are not smooth due to phase transitions. In this respect, our numerical scheme works well. In Sec. 3.2, we will discuss energy releases by the QCD phase transition and find that the values of our interest are $\sim 10^{-2} M_\odot$, for which the numerical accuracy above is certificated mostly. By doubling the mesh points, i.e., $800(r) \times 520(\theta)$, we checked that the order of the magnitude of the released energy does not change.

In constructing one equilibrium sequence, we have three parameters to choose, namely the central density ρ_c , the strength of the magnetic field parameter b , and the axis ratio r_p/r_e . Changing these parameters, we seek solutions in as wide parameter range as possible to study the properties of the equilibrium sequences. We need to calculate more than 50 models changing ρ_c , b , to follow one evolutionary sequence for a fixed baryon mass and magnetic flux. In addition, we change the initial angular momentum of each sequence by 10 models to model the rapidly rotating to the non-rotating case and also 3 different EOSs of mixB200, mixB250, and Shen are employed. This means that we have

to construct at least 1500 models to explore properties of the magnetized compact objects with quark cores systematically. In doing so, we use the Rosenbrock and Gram-Schmidt method, which is helpful to obtain the convergence of the solutions efficiently.

3 NUMERICAL RESULTS

First of all, we discuss how the EOS with the phase transition affects the equilibrium configurations in subsection 3.1, where we pay attention to non-rotating models. Since the magnetars and the high field neutron stars observed so far are all slow rotators, such non-rotating but highly magnetized static models could well be approximated to such stars. Moreover the static models merit that one can see purely magnetic effects on the equilibrium properties because there is no centrifugal force and all the stellar deformation is attributed to the magnetic stress. Then in subsection 3.2, we move on to discuss the the releasable energy of the phase transition from the rotating and magnetized hadronic stars to the hybrid stars.

3.1 Effect of the phase transition on the equilibrium configurations

Now we discuss the equilibrium configurations of the non-rotating and strongly magnetized compact stars with/without the quark cores. Figures 3 and 4 are one example for the hybrid star with mixB200 EOS and for the neutron star with the hadronic ‘‘Shen’’ EOS, showing the distributions of the baryon density (left panel) and the magnetic field (right panel) in the meridional planes, respectively. These two models have the same baryon mass of $1.86M_{\odot}$, and the same magnetic flux of $2.00 \times 10^{30} \text{G cm}^2$, which mean that they are really highly magnetized models with the central magnetic fields of $\sim 10^{18} \text{G}$.

Comparing left panels of Figures 3 and 4, more concentration of the matter in the center is clearly seen for the hybrid star (Figure 3). The concentration is also clearly seen from Figure 5. Inside the inner 6 km of the core of the hybrid star, the mixed phase appears, leading to the enhancement in the compression of the matter due to the softening of the EOS (e.g., Figures 1 and 2).

From right panel of Figure 4, the strong toroidal field lines are seen to behave like a rubber belt, wrapping around the waist of the neutron star. It is found that the magnetic fields frozen-in to the matter, are also compressed by the presence of the quark phase for the hybrid star (right panel of Figure 3). In fact, the pinching of the field lines in the panel corresponds to the surface of the quark core, $\sim 6 \text{km}$ in radius. These qualitative features are also true for the other equilibrium models.

In addition, a general trend in the equilibrium configurations for the hybrid stars is that they are more compact than the neutron star, due to the softness of the EOS. Given the same stellar baryon mass (M_0), the gravitational mass is smaller up to $\sim 0.01M_{\odot}$ than for the neutron stars, reflecting their smaller energy of the quark matter (right panel of Figure 1).

Given the fixed magnetic flux, we can construct equilibrium sequences by changing the central density. To char-

acterize the features of the hybrid stars, we pay attention to the model with the maximum mass ($dM/d\rho_{0,c} = 0$) along each sequence, which we call as the maximum mass sequence for convenience. In table 2, the important physical quantities are summarized for the maximum mass sequences with different magnetic fluxes. It is here noted that the maximum value of the magnetic flux in the table ($\Phi = 2.5 \times 10^{30} \text{G cm}^2$) corresponds to the non-convergence limit, beyond which any solutions cannot converge with the present numerical scheme (Kiuchi & Yoshida 2008). Albeit with such limitations, the field strength is already enough high to affect the configurations and we can well study the magnetic effects on them.

Since the compression of the matter is more enhanced for the smaller bag constant, the hybrid stars with the smaller bag constant become more compact (see R_{cir} Table 2). The maximum magnetic fields are found to become up to about 30 % larger for the hybrid stars than for the neutron stars (compare B_{max} for mixB200 with for Shen). It is also found that the hybrid stars with the smaller bag constant become more prolate (smaller values of \bar{e}) and also their maximum masses become smaller up to $\sim 10\%$ than those for the larger bag constant models. All these features are helpful to understand the properties of the evolution tracks of the hybrid stars, which we discuss from the next section.

3.2 An evolutionary track to a hybrid star

Based on the equilibrium configurations mentioned above, we now move on to discuss an evolutionary path to the formation of a hybrid star due to the spin-down of magnetized and rotating neutron stars.

The evolution scenario we have in mind is illustrated in Figure 6. Let us consider evolution of a single proton-neutron star, left after core-collapse supernova explosion, which rotates with the mass-shedding limit ((A) in Figure 6). The maximum magnetic fields deep inside the core are taken to be $\sim 10^{18} \text{G}$, which could be sustained due to $\alpha - \Omega$ dynamos in such a rapidly rotating neutron star (Thompson & Duncan 1993, 1996). It should be noted that the possibility of such ultra-magnetic fields has not been rejected so far, because what we can learn from the observations of magnetars by their periods and spin-down rates is only their surface fields ($\sim 10^{15} \text{G}$). During their evolution, the baryon mass and the magnetic field strength are assumed to be constant for simplicity. Such models may model the evolution of the isolated compact stars, losing angular momentum via the gravitational radiation and/or magnetic breaking (from (A) to (B)). The phase transition to the hybrid stars is expected to take place during the evolution (shown as (B) to (C) in Figure 6). At the moment, the baryon rest masses and the angular momenta are assumed to be conserved, which may be justified because the timescale of the conversion, albeit uncertain of 0.1-100 s, are too short compared to typical evolutionary timescale of compact stars (more than 10^3 years) (Olesen & Madsen 1991). After the transition, the newly born hybrid star evolves, again losing the angular momentum, to settle down to the magnetized and no-rotating hybrid star finally (see (C) to (D)).

Now using the left panel of Figure 7, we proceed to discuss quantitatively the evolution tracks mentioned above. The red solid the baryon mass ' $M_0 = 1.86M_{\odot}$ ' rotating

Table 2. Global physical quantities for the maximum gravitational mass models of the constant magnetic flux sequences of the non-rotating stars. The order of EOSs from top to down indicates for their hardness from the hadronic "Shen EOS" to the softest "mixB200" EOS.

$\Phi[10^{30}\text{G cm}^2]$	$\rho_{0,c}[10^{15}\text{g/cm}^3]$	$M[M_\odot]$	$M_0[M_\odot]$	$R_{\text{cir}}[\text{km}]$	$B_{\text{max}}[10^{18}\text{G}]$	$H/ W $	$\bar{\epsilon}$
Shen							
0.00E+00	1.16E+00	2.46E+00	2.86E+00	1.35E+01	0.00E+00	0.00E+00	0.00E+00
1.50E+00	1.01E+00	2.45E+00	2.83E+00	1.39E+01	7.34E-01	3.81E-03	-7.40E-03
2.00E+00	1.05E+00	2.45E+00	2.84E+00	1.39E+01	9.83E-01	6.59E-03	-1.30E-02
2.50E+00	1.17E+00	2.46E+00	2.85E+00	1.36E+01	1.26E+00	9.48E-03	-1.86E-02
mixB250							
0.00E+00	1.18E+00	1.83E+00	2.03E+00	1.47E+01	0.00E+00	0.00E+00	0.00E+00
1.50E+00	1.17E+00	1.83E+00	2.02E+00	1.40E+01	9.38E-01	8.28E-03	-1.97E-02
2.00E+00	1.18E+00	1.83E+00	2.02E+00	1.41E+01	1.23E+00	1.45E-02	-3.50E-02
2.50E+00	1.64E+00	1.82E+00	2.00E+00	1.33E+01	1.76E+00	2.02E-02	-4.63E-02
mixB200							
0.00E+00	1.44E+00	1.70E+00	1.88E+00	1.30E+01	0.00E+00	0.00E+00	0.00E+00
1.50E+00	1.29E+00	1.69E+00	1.86E+00	1.34E+01	1.08E+00	9.62E-03	-2.25E-02
2.00E+00	1.35E+00	1.69E+00	1.86E+00	1.34E+01	1.44E+00	1.65E-02	-3.92E-02
2.50E+00	1.65E+00	1.69E+00	1.86E+00	1.31E+01	1.86E+00	2.39E-02	-5.59E-02

with the mass shedding limit (corresponding to (A) in Figure 6). It is noted that the choice of the baryon mass ($M_0 = 1.86M_\odot$) is determined by the maximum mass of the non-rotating hybrid star with the mixB200 EOS as discussed in subsection 3.1 and also that this baryon mass constant sequence has the largest releasable energy at the transition among all the models, as we show this point later. There are many possible paths to convert to hybrid stars with different masses. However, we focused on the maximum energy release with QCD phase transition in this paper. It is possible to select a single equilibrium sequence by keeping the baryon rest mass and the magnetic flux constant simultaneously. Thus the evolution of the proton-neutron star can be described along the line (pink dotted line), going right from one point on the red solid curve. As mentioned, our models assume that all equilibrium sequences begin at their mass-shedding limits and continue to non-rotating equilibrium hybrid stars, at which the sequences end. The final fate is shown by the green dashed line in Figure 7, which is the non-rotating hybrid star with the same baryon mass of ' $M_0 = 1.86M_\odot$ ', here for the mixB200 EOS (corresponding (D) in Figure 6).

Between ρ_1 and ρ_2 (the vertical lines in Figure 7), the phase transition should take place, producing the jump to the sequence of hybrid stars (from (B) to (C) in Figure 6). To see clearly, the transition is shown as the vectors from circle (o) to filled circle (●) in the right panel of Figure 7, which is just the magnification of the left panel near the phase transition. Here, ' $J = 1.00$ ' (' $J = 0.70$ ', ' $J = 0.50$ ', ' $J = 0.25$ ') denotes the angular momentum in unit of $10^{49} \text{ g cm}^2 \text{ s}^{-1}$. We estimate the energy release at the phase transition simply by the difference in the mass-energies between the neutron star and the hybrid star,

$$\Delta M = M_{NS}(M_0, \Phi, J) - M_{HS}(M_0, \Phi, J), \quad (16)$$

with conserving Φ and J through the transition.

In Figure 8, we show the releasable energy of ΔM as a

function of the angular momentum for the mixB200 EOS. Top panel is for the baryon mass of $M_0 = 1.86M_\odot$, which is a special evolutionary track in the sense that the baryon mass is the maximum among non-rotating models, so that the releasable energy is largest among the computed models. Also for the other baryon mass models (middle and bottom panels), it is seen that the energy release becomes smaller for the larger angular momentum. This is simply because stronger centrifugal forces prevent the compression (see the central density (ρ_c) in Tables 3 and 4), making the quark cores smaller, which weakens the effect of the phase transition. In all the computed models, the maximum energy release is found to be $\lesssim 0.01M_\odot$. This energy is equivalent to $\lesssim 2 \times 10^{52}$ erg, which is truly larger compared with the energies of supernovae ($\sim 10^{51}$ erg), however much smaller than those previously estimated ($\sim 10^{53}$ erg) in which the conversion to the strange quark star is assumed (Gourgoulhon et al. 1999; Yasutake et al. 2005; Zdunik et al. 2007). We note that ΔM becomes less than $\Delta M \lesssim 10^{-3}M_\odot$ for the larger bag constant models of mixB250. This is because the large bag constant suppresses the conversion from hadron matter to quark matter as already mentioned. Unfortunately, exact values of ΔM for the mixB250 models cannot be found by the present scheme because ΔM becomes more than 3 orders-of-magnitude smaller than M , while M can be estimated at most with the numerical accuracy of 10^{-2} for this case. This is also the case for small baryon mass cases (see the bottom panel of Figure 8). For getting more precise solutions, we may need to employ the so-called spectral method. Although the LORENE code (Bonazzola et al. 1998) employs the method, it cannot treat the magnetic fields yet. The implementation of the method is still a major undertaking, which we pose as a next task of this paper.

Other numerical values characterizing the phase transition are given in Tables 3 and 4. Table 4 is for the non-magnetized models, which is given for comparison. For models with smaller angular momentum (J in the tables), it can

be readily seen that the gravitational masses (M) and the circumferential radii (R_{cir}) become smaller, while the central baryon densities ($\rho_{0,c}$) and the maximum strength of the magnetic fields (B_{max}) become larger, all simply due to the smaller centrifugal forces. If the newly-born neutron star evolve to the non-rotating neutron star without experiencing the conversion, the increase of the central density is less than $\sim 20\%$ (compare $\rho_{0,c}$ of "Shen" at the mass shedding limit with the one at no-rotating limit in Table 3). On the other hand, the maximum density is found to increase about several times larger by the phase transition (compare $\rho_{0,c}$ between "Shen" with "mixB200" in Table 3). Frozen-in to the matter, the maximum magnetic field increases up to 50% while the change is an order of unit percent in absence of the conversion (see Figure 9). Due to the conservation of angular momentum, the angular velocity increases about $\Delta\Omega/\Omega \sim 30\%$ after the conversion (see Figure 10 and Tables 3). Also in this case, it is noted that the spin-up is suppressed for the larger bag constant models (see Table 3). We speculate that such spin-up, much larger than the canonical glitches of magnetars ($\Delta\Omega/\Omega \sim 10^{-7}$, Woods & Thompson (2006)), could be new observable signatures, marking the occurrence of the phase transition.

4 SUMMARY AND DISCUSSION

In this study, we investigated structures of general relativistic hybrid stars containing super-strong magnetic fields. Pushed by the results of recent stellar evolution calculations and the outcomes of recent MHD simulations of core-collapse supernovae, we treated the toroidal fields only. Using the bulk Gibbs construction, we modeled the EOS with a first order transition by bridging the MIT bag model for the description of quark matter and the nuclear EOS by Shen et al. We found that the presence of the quark phase can affect the distribution of the magnetic fields inside the hybrid stars, leading to the enhancement of the field strength about 30 % than for the normal neutron stars. Using the equilibrium configurations, we explored the possible evolutionary paths to the formation of hybrid stars due to the spin-down of magnetized and rotating neutron stars. For simplicity, the total baryon mass and magnetic flux are taken to be conserved during the evolution but that the angular momenta are lost gravitational waves and/or magnetic breaking. We found that the energy release by the conversion to hybrid stars is typically $\lesssim 10^{52}$ erg, smaller than previously estimated for the conversion to the strange quark stars.

In association with the vast energy release, it is natural to expect the emissions of gravitational waves. Amplitude of the gravitational waves associated with the phase transition, h , is given as follows (Pacheco 1998),

$$h \sim 2 \left(\frac{G\alpha E_{\text{tot}}}{c^3\tau} \right)^{1/2} \frac{1}{r\omega}. \quad (17)$$

Here, E_{tot} , α , τ , r , and ω are energy release, fraction of the energy release emitted in form of the gravitational waves, damping time scale of the gravitational wave, distance to the source, and angular velocity, respectively. To set an absolute upper bound, we could choose $E_{\text{tot}} \sim 10^{52}$ erg and $\omega \sim 100$ rad s $^{-1}$ according to Table 3. We assume that the source is in our galactic center of $r \sim 10$ kpc and that the

damping timescale and α is ~ 100 ms and 10^{-4} , respectively inferred from Abdikamalov et al. (2008). The resulting amplitudes become as high as $h \sim 10^{-18\sim-19}$ peaking at \sim kHz, which are surely within the detection limits for the laser interferometers on line such as LIGO, VIRGO, GEO600, and TAMA300. Considering the optimal sensitivity of the interferometers of $h \sim 10^{-21}$ at ~ 1 KHz, such signals, far stronger than the ones from canonical core-collapse supernovae (e.g., Kotake et al. (2009a,b); Murphy et al. (2009)), are possibly visible for a source out to Megaparsec distances. In combination with the signatures of the spin-up discussed before, we speculate that the waveforms of such strong gravitational waves could provide us hints of properties of QCD phase transition. To find the accurate waveforms, general relativistic simulations are indispensable (Kiuchi et al. in preparation). Moreover accurate predictions for neutrino emissions (Gentile et al. 1993; Nakazato et al. 2008; Sagert et al. 2008) and their detectability are remained to be studied (e.g., Kawagoe et al. (2009)). This paper should help to construct the initial conditions for such studies.

Alcock et al. (1986) claimed that the conversion from the hadronic to the mixed phase occurs instantaneously in the weak interaction timescales (such as $d + u \leftrightarrow s + u$) when the central density exceeds the critical value of ρ_1 in Figures 1 and 2. If so, the newly-born neutron stars may convert to the hybrid stars in the postbounce phase, before they evolve from A to B illustrated in Figure 6. In this case, the released energy may be used to power original core-collapse supernovae or more energetic supernovae such as hypernovae. Although the formation paths to hybrid stars are different from the ones discussed in this paper, the estimation method of the energy release here are also applicable if we implement the EOS at finite temperature and high lepton fraction (Yasutake & Kashiwa 2009), which we plan to study as a sequel to this paper.

It has been pointed out that the super-strong magnetic field more than 10^{18} G can affect the stiffness of the EOS (Broderick et al. 2000). As mentioned, the maximum magnetic field increases about $\sim 30\%$ by the phase transition, while it increases only unit percent if the compact stars evolve to the non-rotating ones in absence of the transition. This suggests that the magnetic effects should be seriously taken into account to our models treating the phase transition. Especially for the quark phase, Fukushima & Warringa (2008); Noronha et al. (2007) have recently found that the energy gaps of magnetic color-flavor-locked phase are oscillating functions of the magnetic field. Such effects are remained to be studied.

We should comment about the very high values of the magnetic fields, larger than 10^{18} G. Ruderman et al. (2000) suggested that such high magnetic fields can be brought to the stellar surface by buoyancy forces. According to their result, we estimate the buoyancy time scale in our models. The buoyancy force can be expressed as

$$F_b \sim \frac{B_\phi^2}{8\pi c_s^2} g, \quad (18)$$

where c_s and g are the sound speed and the gravitational acceleration, respectively. Putting typical values inside compact objects into the equation, we roughly estimate the time

Table 3. Global physical quantities for the equilibrium sequences of the rotating stars with $M_0 = 1.86M_\odot$, $\Phi_{30} = 2.00$.

EOS	$\rho_{0,c}[10^{15}\text{g/cm}^3]$	$M[M_\odot]$	$R_{\text{cir}}[\text{km}]$	$\Omega [10^3 \text{ rad/s}]$	$T/ W $	$H/ W $	\bar{e}	$B_{\text{max}}[10^{18}\text{G}]$
Shen(MS)	4.11E-01	1.73E+00	2.22E+01	1.59E+00	9.41E-02	2.89E-02	2.00E-01	9.61E-01
$J = 1.00 \times 10^{49} \text{ g cm}^2/\text{s}$								
Shen	4.51E-01	1.72E+00	1.70E+01	8.73E-01	3.69E-02	2.47E-02	5.40E-02	9.65E-01
mixB250	5.11E-01	1.72E+00	1.69E+01	9.31E-01	3.65E-02	2.42E-02	5.40E-02	9.68E-01
mixB200	8.26E-01	1.71E+00	1.61E+01	1.30E+00	3.78E-02	2.11E-02	7.01E-02	1.10E+00
$J = 0.75 \times 10^{49} \text{ g cm}^2/\text{s}$								
Shen	4.63E-01	1.71E+00	1.64E+01	6.69E-01	2.15E-02	2.37E-02	7.26E-03	9.70E-01
mixB250	5.56E+00	1.71E+00	1.63E+01	7.40E-01	2.13E-02	2.33E-02	8.32E-03	9.74E-01
mixB200	9.63E-01	1.71E+00	1.51E+01	1.10E+00	2.24E-02	1.93E-02	2.74E-02	1.20E+00
$J = 0.50 \times 10^{49} \text{ g cm}^2/\text{s}$								
Shen	4.72E-01	1.71E+00	1.60E+01	4.54E-01	9.83E-03	2.31E-02	-3.05E-02	9.70E-01
mixB250	5.93E-01	1.71E+00	1.59E+01	5.16E-01	9.77E-03	2.24E-02	-2.82E-02	9.75E-01
mixB200	1.08E+00	1.70E+00	1.43E+01	8.07E-01	1.04E-02	1.81E-02	-8.49E-03	1.31E+00
$J = 0.25 \times 10^{49} \text{ g cm}^2/\text{s}$								
Shen	4.79E-01	1.71E+00	1.58E+01	2.28E-01	4.53E-03	2.28E-02	-4.82E-02	9.70E-01
mixB250	6.15E-01	1.71E+00	1.57E+01	2.60E-01	4.43E-03	2.20E-02	-4.57E-02	9.75E-01
mixB200	1.21E+00	1.69E+00	1.42E+01	4.39E-01	2.82E-03	1.71E-02	-3.15E-02	1.39E+00
no rotation								
Shen	4.86E-01	1.71E+00	1.57E+01	0.00E+00	0.00E+00	2.25E-02	-6.35E-02	9.72E-01
mixB250	6.36E-01	1.71E+00	1.55E+01	0.00E+00	0.00E+00	2.16E-02	-6.03E-02	9.75E-01
mixB200	1.35E+00	1.69E+00	1.34E+01	0.00E+00	0.00E+00	1.65E-02	-3.92E-02	1.44E+00

Table 4. Same as Table 3 but for $\Phi_{30} = 0$.

EOS	$\rho_{0,c}[10^{15}\text{g/cm}^3]$	$M[M_\odot]$	$R_{\text{cir}}[\text{km}]$	$\Omega [10^3 \text{ rad/s}]$	$T/ W $	\bar{e}
Shen(MS)	3.81E-01	1.74E+00	2.10E+01	1.45E+00	1.12E-01	2.79E-01
$J = 1.00 \times 10^{49} \text{ g cm}^2/\text{s}$						
Shen	4.40E-01	1.72E+00	1.66E+01	8.08E-01	3.58E-02	1.07E-01
mixB250	4.62E-01	1.72E+00	1.66E+01	8.30E-01	3.54E-02	1.06E-01
mixB200	7.80E-01	1.71E+00	1.58E+01	1.18E+00	3.72E-02	1.11E-01
$J = 0.75 \times 10^{49} \text{ g cm}^2/\text{s}$						
Shen	4.51E-01	1.71E+00	1.61E+01	6.23E-01	2.09E-02	6.49E-02
mixB250	5.16E-01	1.71E+00	1.61E+01	6.69E-01	2.07E-02	6.43E-02
mixB200	9.02E-01	1.70E+00	1.49E+01	1.01E+00	2.18E-02	6.90E-02
$J = 0.50 \times 10^{49} \text{ g cm}^2/\text{s}$						
Shen	4.61E-01	1.71E+00	1.58E+01	4.25E-01	9.54E-03	3.06E-02
mixB250	5.51E-01	1.71E+00	1.57E+01	4.69E-01	9.49E-03	3.04E-02
mixB200	1.03E+00	1.70E+00	1.42E+01	7.51E-01	1.02E-02	3.33E-02
$J = 0.25 \times 10^{49} \text{ g cm}^2/\text{s}$						
Shen	4.67E-01	1.71E+00	1.56E+01	2.15E-01	2.54E-03	8.48E-03
mixB250	5.74E-01	1.71E+00	1.55E+01	2.42E-01	2.52E-03	8.46E-03
mixB200	1.14E+00	1.69E+00	1.37E+01	4.08E-01	2.65E-03	9.10E-03
no rotation						
Shen	4.75E-01	1.71E+00	1.55E+01	0.00E+00	0.00E+00	0.00E+00
mixB250	5.82E-01	1.71E+00	1.54E+01	0.00E+00	0.00E+00	0.00E+00
mixB200	1.19E+00	1.69E+00	1.35E+01	0.00E+00	0.00E+00	0.00E+00

scale τ as

$$\tau \sim 10^{-3} - 10^{-4} \text{s} \left(\frac{\rho}{10^{15} \text{g/cm}^3} \right)^{1/2} \left(\frac{R}{10^6 \text{cm}} \right)^{1/2} \left(\frac{c_s}{10^{10} \text{cm/s}} \right) \left(\frac{B_\phi}{10^{18} \text{G}} \right)^{-1} \left(\frac{g}{10^{14} \text{cm/s}^2} \right)^{-1/2}, \quad (19)$$

where R is the typical size of compact stars. Clearly such magnetic fields are not stable against the buoyancy forces in stellar evolution time scale $\sim 10^3$ yr. Based on the MHD simulations in full general relativity, Kiuchi et al. (2008c) recently showed that the toroidal configurations of neutron stars is really dynamically unstable due to the buoyant instability. But more important finding relevant to this study, is that the toroidal magnetic fields settle down to a new equilibrium state with the circular motions in the meridian plane. In the new equilibrium configurations, the toroidal fields almost equivalent to the strength before the onset of the instability, are expected to be much stronger than the poloidal ones. This suggests that our models presented here, albeit unstable to the buoyant instability, could be helpful to understand equilibrium configurations of magnetized hybrid stars. Such stability analysis is an important issue yet to be studied.

Our treatments of the phase transition should be more sophisticated. We plan to employ the so-called NJL model (e.g., Yasutake & Kashiwa (2009)) instead of the simple MIT bag model. Moreover we shall take into account finite size effects (Maruyama et al. 2006) such as quark-nuclear pasta structures. We considered cold compact objects, namely with zero-temperature and zero-neutrino fraction. We plan to extend this study to the finite temperature with the non-zero neutrino fraction, which should be useful for studying earlier evolutions of compact stars soon after their formation.

The evolution sequence we explored is a very simplified one. For more realistic estimations, one needs the two dimensional evolutionary calculation in full general relativistic framework, not an easy job, due to the treatment of convection, combustion, cooling and/or heating processes, nucleosynthesis on the surface, and so forth. Applying the method recently reported by Pons et al. (2008), we think that we could study the magneto-thermal evolution of neutron stars to the hybrid stars. By doing so, we hope to investigate the peculiar properties in the light curves, which has been pointed out to be another observationally visible (Page et al. 2000; Blaschke et al. 2000, 2001; Grigorian et al. 2005). All of such studies should be indispensable to pave the way for the understanding of the long-veiled phase-transition physics from the astrophysical phenomena.

ACKNOWLEDGMENTS

We are grateful to Shijun Yoshida, Y. Eriguchi, and M. Hashimoto, for informative discussions. N.Y. thanks to Y. Sekiguchi for stimulating discussions. K.K. is grateful to K. Sato and S. Yamada for continuing encouragements. Numerical computations were in part carried on XT4 general common use computer system at the center for Computational Astrophysics, CfCA, the National Astronomical Observatory of Japan. This study was supported in part by the Grants-in-Aid for the Scientific Research from the Ministry of Education, Science and Culture of Japan (No. S19104006, 20740150, 21105512).

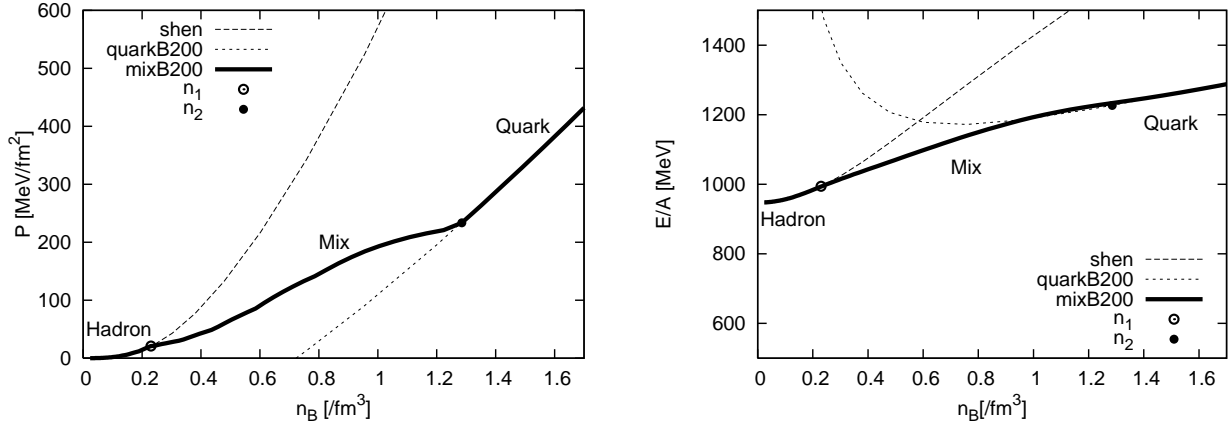


Figure 1. The constructed EOS under bulk Gibbs condition. The labels of “quarkB200” and “mixB200” indicate a pure quark matter EOS and an EOS with mixed phase with $B = 200 \text{ MeV fm}^{-3}$, whereas “Shen” indicates Shen EOS of pure hadronic matter. Left and right panels are the pressure and the energy per baryon as a function of the baryon density, respectively.

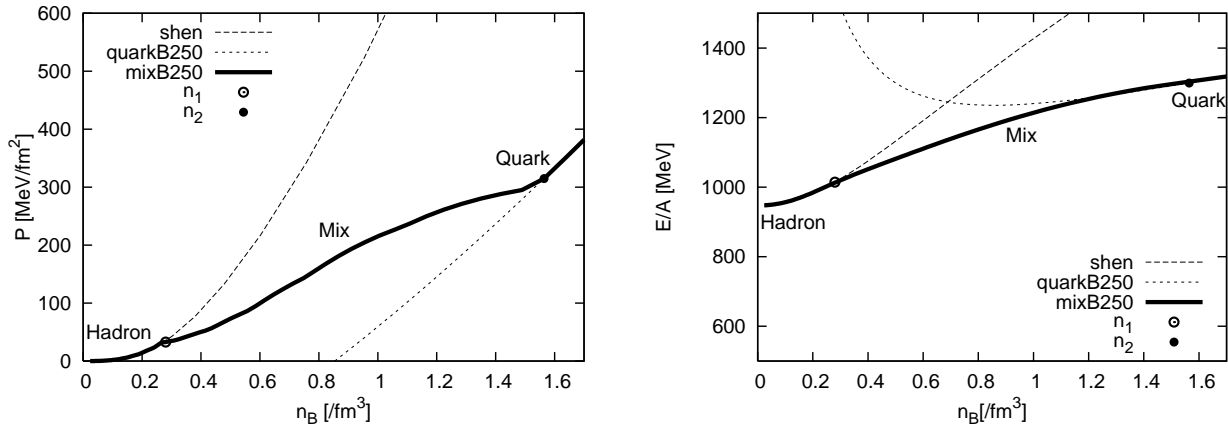


Figure 2. Same as Figure 1 but for $B = 250 \text{ MeV fm}^{-3}$.

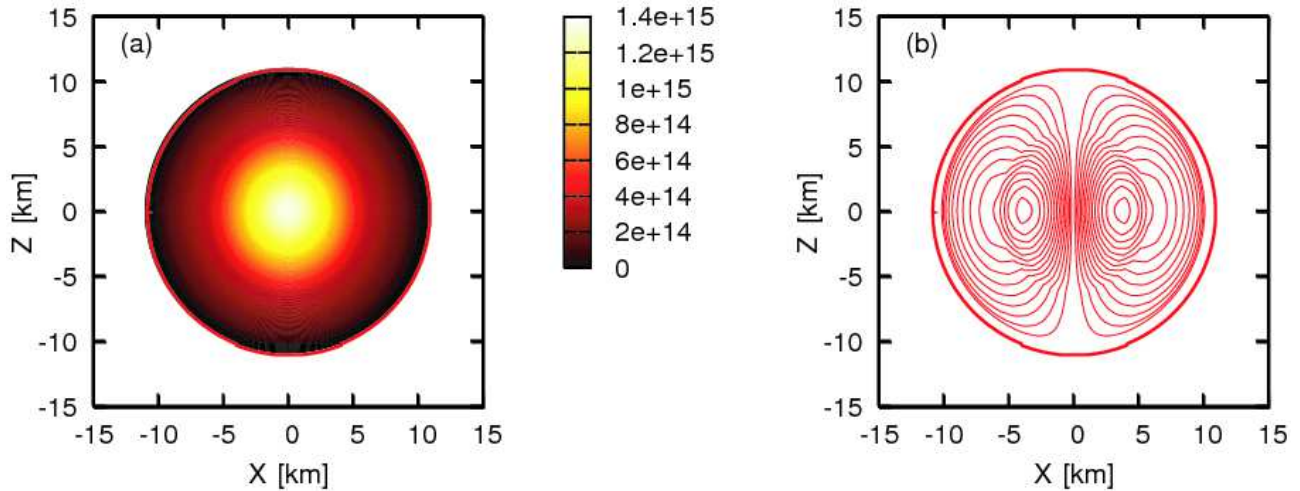


Figure 3. Distribution of (a): baryon density [g/cm^3] and (b): magnetic field with “mixB200” EOS. Here, the central baryon density $\rho_{0,\text{max}} = 1.35 \times 10^{15} \text{ g cm}^{-3}$, the baryon mass $M_0 = 1.86M_\odot$, the gravitational mass $M = 1.69M_\odot$, the flux normalized by units of 10^{30} G cm^2 , $\Phi_{30} = 2.00$, the ratio of the magnetic energy to the gravitational energy, $H/|W| = 1.65 \times 10^{-2}$, maximum magnetic fields, $B_{\text{max}} = 1.44 \times 10^{18} \text{ G}$.

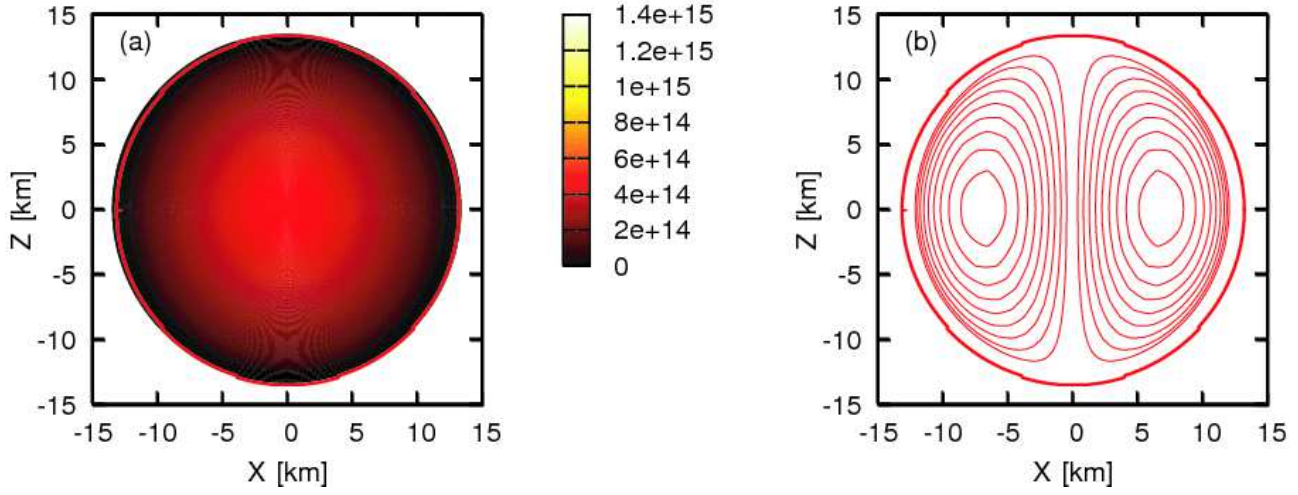


Figure 4. Same as Figure 4 but for hadronic "Shen" EOS, $M_0 = 1.86M_\odot$ star with the central baryon density $\rho_{0,\max} = 4.86 \times 10^{14} \text{ g cm}^{-3}$, $M = 1.71M_\odot$, $H/|W| = 2.25 \times 10^{-2}$, $B_{\max} = 0.97 \times 10^{18} \text{ G}$.

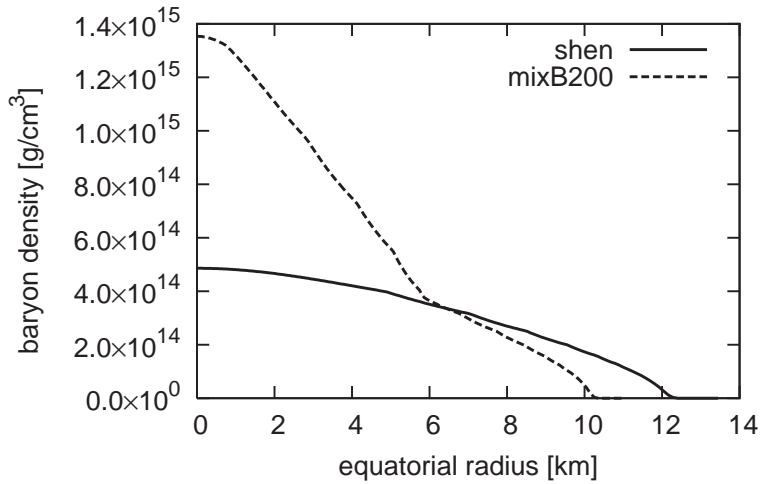


Figure 5. Distribution of baryon density for Figure 3 and Figure 4.

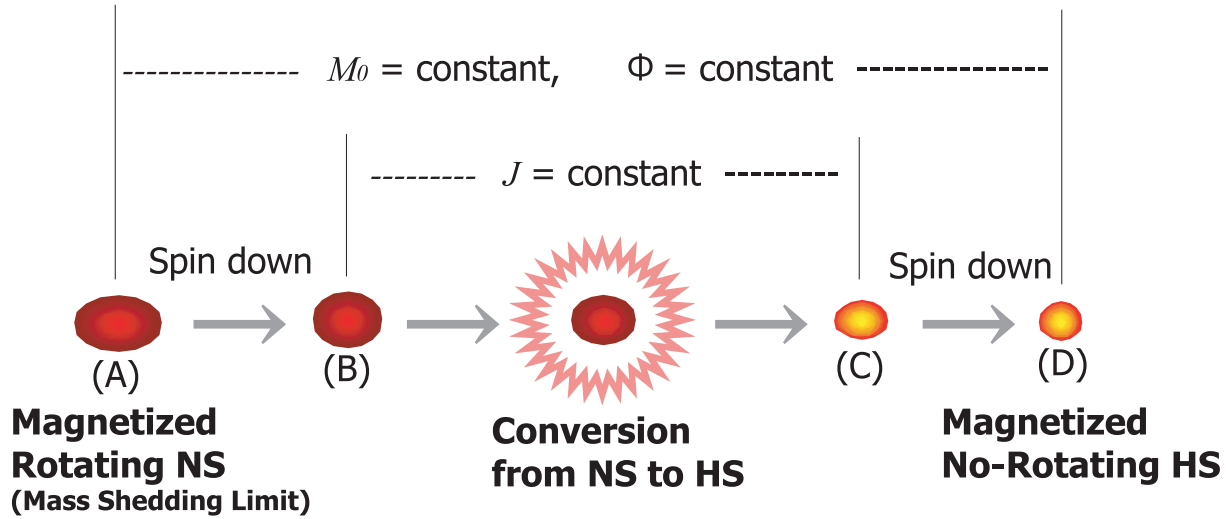


Figure 6. Schematic drawing, showing our scenario of conversion from neutron stars (NSs) to hybrid stars (HSs). The baryon rest mass and the magnetic flux are assumed to conserve for modeling the isolated neutron stars that are adiabatically losing angular momentum via the gravitational radiation and/or magnetic braking. We furthermore assume the conservation of the angular momentum at the conversion.

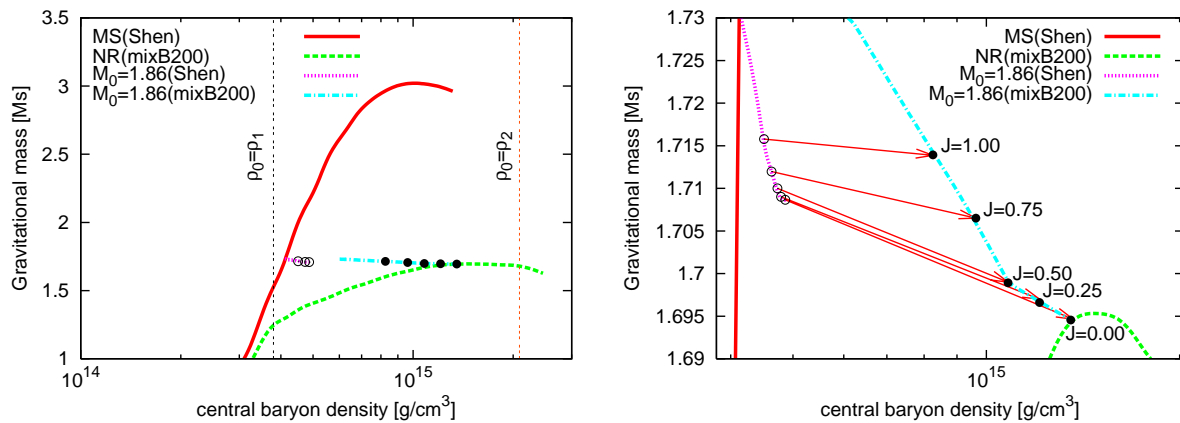


Figure 7. Gravitational masses versus central effective baryon densities at the constant magnetic flux, $\Phi_{30} = 2.00$. The right panel is magnified figure of the left panel. The solid line of MS(Shen) is for mass shedding limits of neutron stars. The dashed line of NR(mixB200) is for no-rotating hybrid stars with "mixB200" EOS. The line of ' $M_0 = 1.86$ (Shen)' is one example in all baryon mass constant lines for neutron stars. ' $M_0 = 1.86$ (mixB200)' is same as ' $M_0 = 1.86$ (Shen)', but for hybrid stars. Conversions from neutron stars to hybrid stars are shown as the vectors from circle (\circ) to filled circle (\bullet). Here, J is the angular momentum in unit of $10^{49} \text{ g cm}^2 \text{ s}^{-1}$. The lines of ρ_1 and ρ_2 are critical densities of phase equilibrium for hadron phase and quark phase shown in Figure 1. and Table 1.

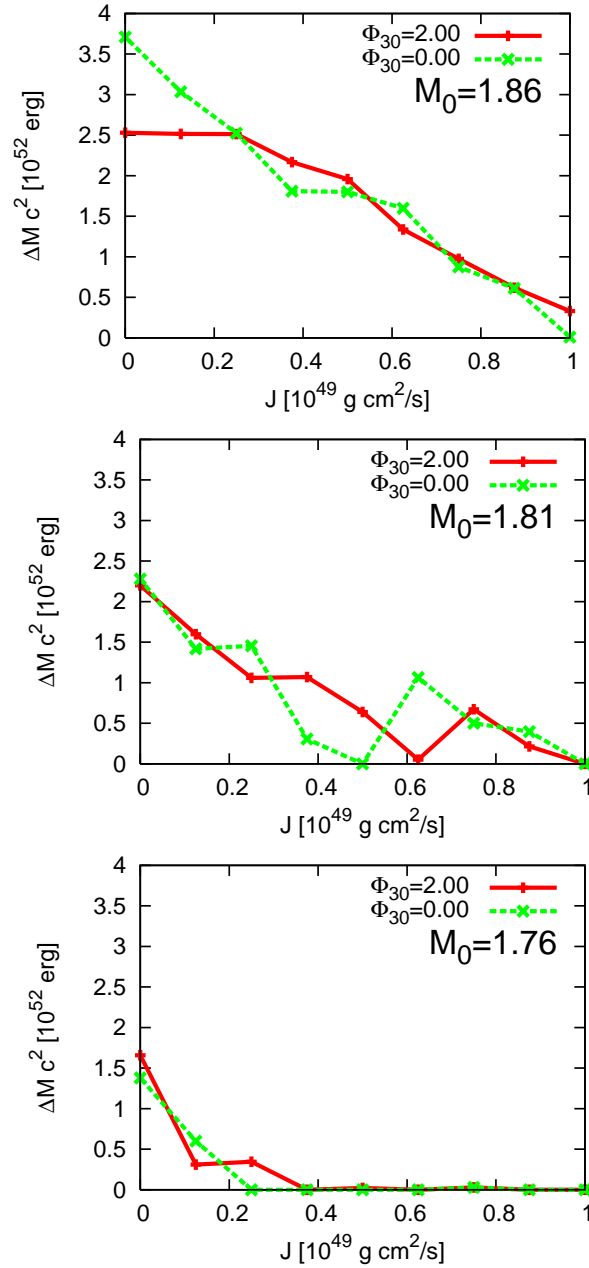


Figure 8. Energy release (ΔM) as a function of the angular momentum (J) at the moment of the phase transition for magnetized ($\Phi_{30} = 2.00$) and non-magnetized models ($\Phi_{30} = 0$) for $M_0 = 1.86M_\odot$ (the upper panel), $M_0 = 1.81M_\odot$ (the middle panel), and $M_0 = 1.76M_\odot$ (the lower panel). Note here that these are the case for the mixB200 EOS. For the mixB250 EOS, exact values of ΔM cannot be estimated due to the limitation of the present scheme. Unfortunately it is also seen here, for example, for the case of smaller baryon mass for $J \gtrsim 0.4 \times 10^{49}[\text{g cm}^2 \text{ s}^{-1}]$ (bottom)(see text for more details).

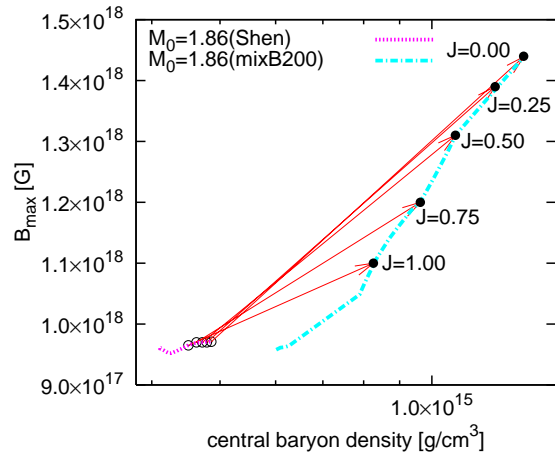


Figure 9. Central baryon density versus maximum magnetic field for same stars of Figure 7.

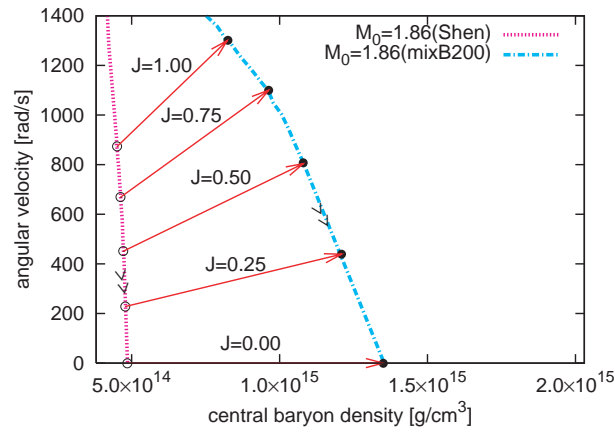


Figure 10. Central baryon density versus angular velocities for same stars of Figure 7. Angular velocities are monotonically decreased without the conversion, shown as '>>'.>>

REFERENCES

- Abdikamalov, E. B., Dimmelmeier, H., Rezzolla, L., and Miller, J. C., 2009, *MNRAS*, 392, 52A
- Akmal, A., Pandharipande, V. R., and Ravenhall, D. G. 1998, *Phys. Rev. C*, 58, 1804
- Alcock, C., Farhi, E., and Olinto, A., 1986, *ApJ*, 310, 261
- Alcock, C., & Olinto, A. 1988, *Annual Review of Nuclear and Particle Science*, 38, 161
- Alford, M., Blaschke, D., Drago, A., Klähn, T., Pagliara, G., & Schaffner-Bielich, J. 2007, *Nat.*, 445, 7
- Berezhiani, Z., Bombaci, I., Drago, A., Frontera, F., & Lavagno, A. 2003, *ApJ*, 586, 1250
- Benvenuto, O. G., Vucetich, H., & Horvath, J. E. 1994, *MNRAS*, 266, 690
- Benvenuto, O.G., and Horvath, J. E., 1989, *Phys. Rev. Lett.*, 63, 716
- Blaschke, D., Klähn, T., and Voskresensky, D. N., 2000, *ApJ*, 533, 406
- Blaschke, D., Grigorian, H., and Voskresensky, D., 2001, *A&A*, 368, 561
- Bombaci, I., & Datta, B. 2000, *ApJL*, 530, L69
- Bombaci, I., Panda, P. K., Providencia, C., and Vidana, I., 2008, *Phys. Rev. D*, 77, 083002
- Bonazzola, S. & Gourgoulhon, E. 1994, *CQG*, 11, 1775
- Bonazzola, S., Gourgoulhon, E., & Marck, J.-A. 1998, *Phys. Rev. D*, 58, 104020
- Bodmer, A. R., 1971, *Phys. Rev. D*, 4, 160
- Braithwaite, J., & Spruit, H. C., 2004, *nat.*, 431, 820
- Broderick, A., Prakash, M., and Lattimer, J. M., 2000, *ApJ*, 537, 351
- Burgio, G. F., Schulze, H. J., and Weber, F., 2003, *A&A*, 408, 675
- Burrows, A & Lattimer, J. M. 1986, *ApJ*, 307, 178
- Chodos, A., Jaffe, R. L., Johnson, K., Thorn, C. B., & Weisskopf, V. F. 1974, *Phys. Rev. D*, 9, 3471
- Chau, H. F. 1997, *ApJ*, 479, 886
- Cook, G. B., Shapiro, S. L., and Teukolsky, S. A., 1992, *ApJ* 398, 203; 1994, *ApJ*, 422, 227.
- Douchin, F., & Haensel, P., 2001, *A&A*, 380, 151
- Drago, A., Lavagno, A., and Parenti, I., 2007, *ApJ*, 659, 1519.
- Drago, A., Lavagno, A., & Pagliara, G. 2004, *Phys. Rev. D*, 69, 057505
- Endo, T., Murayama, T, Chiba, S., and Tatsumi, T., 2006, *Prog. Theor. Phys.*, 115, 337
- Fukushima, K. & Warringa, H. J., 2008, *Phys. Rev. Lett.*, 100, 032007.
- Gentile, N. A., Aufderheide, M. B., Mathews, G. J., Swesty, F. D., & Fuller, G. M. 1993, *ApJ*, 414, 701
- Glendenning, N. K. 1992, *Phys. Rev. D*, 46, 1274
- Glendenning, N. K., 2001, *Physic. Rep.*, 342, 393
- Grigorian, H., Blaschke, D., and Voskresensky, D., 2005, *Phys.Rev.C* 71, 045801
- Gourgoulhon, E., Haensel, P., Livine, R., Paluch, E., Bonazzola, S., and Marck, J.-A., 1999, *A&A*, 349, 851
- Goldreich, P. & Reisenegger, A., 1992, *ApJ*, 395, 250
- Heger, A., Woosley, S. E., and Spruit, H. C., 2005, *ApJ* 626, 350
- Haensel, P., Zdunik, J. L., & Schaeffer, R. 1986, *A&A*, 160, 251
- Heger, A., Woosley, S. E., and Spruit, H. C., 2005, *ApJ*, 626, 350
- Horvath, J. E., 2007, *astro-ph/0703233*
- Itoh, N., 1970, *Prog. Theor. Phys.*, 44, 291
- Ioka, K., 2001, *MNRAS*, 327, 639
- Ivanov, Y. B., Khvorostukhin, A. S., Kolomeitsev, E. E., Skokov, V. V., Toneev, V. D., and Voskresensky, D. N., 2005, *Phys. Rev. D*, 72, 025804
- Kawagoe, S., Takiwaki, T., & Kotake, K. 2009, *arXiv:0906.3180 JCAP* in press
- Kiuchi, K., & Kotake, K., 2008, *MNRAS*, 385, 1327
- Kiuchi, K., & Yoshida, S., 2008, *Phys. Rev. D*, 78, 4045
- Kiuchi, K., Shibata, M., and Yoshida, S. 2008, *Phys. Rev. D*, 78, 4029
- Kiuchi, K., Kotake, K., & Yoshida, S. 2009, *ApJ*, 698, 541
- Komatsu, H., Eriguchi, Y., and Hachisu, I., 1989, *MNRAS*, 237, 355; 239, 153.
- Kotake, K., Sawai, H., Yamada, S., and Sato, K., 2004, *ApJ*, 608, 391
- Kotake, K., Sato, K., & Takahashi, K. 2006, *Reports of Progress in Physics*, 69, 971
- Kotake, K., Iwakami, W., Ohnishi, N., & Yamada, S. 2009, *ApJ*, 697, L133
- Kotake, K., Iwakami, W., Ohnishi, N., & Yamada, S. 2009, *ApJ*, 704, 951
- Lattimer, J. M. & Prakash, M. 2007 *Phys. Rept.* 442, 109
- Lin, L. M., Cheng, K. S., Chu, M. C., and Suen, W. M., 2006, *ApJ*, 639, 382
- Livne, E., Dessart, L., Burrows, A. and Meakin, C. A., 2007, *ApJS*, 170, 187
- Bonanno, L., Drago, A., & Lavagno, A. 2007, *Phys. Rev. Lett.*, 99, 242301
- Lugones, G., Benvenuto, O. G., and Vucetich, H., 1994, *Phys. Rev. D*, 50, 6100
- Dessart, L., Burrows, A., Livne, E., & Ott, C. D. 2007, *ApJ*, 669, 585
- Lyne, A. G., & Graham-Smith, F. 2005, *Pulsar Astronomy*, by Andrew G. Lyne and Francis Graham-Smith, pp. . ISBN 0521839548. Cambridge, UK: Cambridge University Press, 2005.,
- Madsen, J. 2000, *Phys. Rev. Lett.*, 85, 10
- Mallick, R., Ghosh, S. K., Raha, S., 2009, *astro-ph/09043393*
- Maruyama, T., Tatsumi, T., Voskresensky, D. N., Tanigawa, T., Endo, T., & Chiba, S. 2006, *Phys. Rev. C*, 73, 035802
- Murphy, J. W., Ott, C. D., & Burrows, A. 2009, *arXiv:0907.4762*
- Muto, T., & Tatsumi, T. 1990, *Prog. Theor. Phys.*, 83, 499
- Nakazato, K., Sumiyoshi, K., and Yamada, S., 2008, *Phys. Rev. D*, 77, 103006
- Noronha, J. L., and Shovkovy, I. A., 2007, *Phys. Rev. D*, [A 76, 105030
- Obergaulinger, M., Aloy, M. A., and Müller, E., 2006, *A&A*, 450, 1107
- Olesen, M. I., & Madsen, J., 1991, *Nuc. Phys. B Suppl.*, 24B, 170
- Pacheco, J. A. D., 1998, *A&A*, 336, 397
- Page, D., Prakash, M., Lattimer, J. M., and Steiner, A. W., 2000, *Phys. Rev. Lett.*, 85, 2048
- Pons, J. A., Miralles, J. A., & Geppert, U. 2008, *arXiv:0812.3018*
- Ransom, S. M., Hessels, J. W. T., Stairs, I. H., Freire, P.

- C. C., Camilo, F., Kaspi, V. M., and Kaplan, D. L., 2005, *Science*, 307, 892
- Ruderman, M. A., Tao, L., and Kluzniak, W., 2000, *ApJ*, 542, 243
- Sagert, I., Hempel, M., Pagliara, G., Schaffner-Bielich, J., Fischer, T., Mezzacappa, A., Thielemann, F. K., and Liebendörfer, M., 2008, astro-ph/0809.4225
- Sawai, H., Kotake, K. and Yamada, S., 2008, *ApJ*, 672, 465
- Senger, P. 2004, *Journal of Physics G Nuclear Physics*, 30, 1087
- Shapiro, S. L., & Teukolsky, S.A., 1983, Research supported by the National Science Foundation. New York, Wiley-Interscience 1983, 645p.
- Shen, H., Toki, H., Oyamatsu, K., and Sumiyoshi, K., 1998, *Nucl. Phys. A*, 637, 435.
- Stephanov, M., 2004, *Prog. Theor. Phys. Suppl.* 153, 139
- Takahara, M., & Sato, K. 1985, *Phys. Lett. B*, 156, 17
- Takiwaki, T., Kotake, K., Nagataki, S., & Sato, K. 2004, *ApJ*, 616, 1086
- Takiwaki, T., Kotake, K., & Sato, K. 2009, *ApJ*, 691, 1360
- Thompson, C. & Duncan, R. C. 1993, *ApJ*, 408, 194
- Thompson, C. & Duncan, R. C. 1996, *ApJ* 473, 322
- Watts, A. L., & Reddy, S. 2007, *MNRAS*, 379, L63
- Weber, F. 1999, *Pulsars as astrophysical laboratories for nuclear and particle physics* /F. Weber. Bristol, U.K. : Institute of Physics, c1999. QB 464 W42 1999.
- Wald, R. M., 1984, *General Relativity* (The University of Chicago Press)
- Wiringa, R. B., Filks, V., and Fabrocini, A. 1988, *Phys. Rev. C*, 38, 1010
- Witten, E., 1984, *Phys. Rev. D*, 30, 272
- Woods, P. M., & Thompson, C. 2006, *Compact stellar X-ray sources*, 547
- Yasutake, N., Hashimoto, M., and Eriguchi. Y., 2005, *Prog. Theor. Phys.*, 113, 953
- Yasutake, N., Kotake, K., Hashimoto, M., and Yamada, S., 2007, *Phys. Rev. D*, 75, 084012
- Yasutake, N., Kashiwa, K., 2009, *Phys. Rev. D*, 79, 043012
- Zdunik, J. L., Haensel, P., & Schaeffer, R. 1987, *A&A*, 172, 95
- Zdunik, J. L., Bejger, M., Haensel, P., and Gourgoulhon, E., 2007, *A&A*, 465, 533
- Zdunik, J. L., Bejger, M., Haensel, P., & Gourgoulhon, E. 2008, *A&A*, 479, 515

This paper has been typeset from a \TeX / \LaTeX file prepared by the author.